JVSTA
JOURNAL OF VACUUM SCIENCE AND TECHNOLOGY A

Effects of ioninduced electron emission on magnetron plasma instabilities

M. B. Hendricks, P. C. Smith, D. N. Ruzic, A. Leybovich, and J. E. Poole

Citation: J. Vac. Sci. Technol. A **12**, 1408 (1994); doi: 10.1116/1.579329
View online: http://dx.doi.org/10.1116/1.579329
View Table of Contents: http://avspublications.org/resource/1/JVTAD6/v12/i4
Published by the AVS: Science & Technology of Materials, Interfaces, and Processing

Effects of ion-induced electron emission on magnetron plasma instabilities

M. B. Hendricks, P. C. Smith, and D. N. Ruzic
University of Illinois, Urbana, Illinois 61801

A. Leybovich and J. E. Poole
TOSOH SMD, Inc., Grove City, Ohio 43123

(Received 15 November 1993; accepted 15 April 1994)

Some magnetron sputtering systems experience rapid oscillations in the current and voltage of the plasma discharge after several hours when equipped with certain targets. These oscillations often lead to the plasma becoming extinguished, a condition known as "flame-out." This article details the study of two 90% W–10% Ti magnetron targets which differed in density. The higher density targets sometimes experienced flame-out after approximately 3 h of sputtering. The less dense material could be sputtered for the entire 15 h life of the target. Scanning electron microscopy pictures and atomic composition depth profiles were obtained using Auger electron spectroscopy. In addition, a Colutron-based ion source with a high vacuum system was used to measure ion-induced secondary electron emission coefficients as a function of energy, ion specie, and gas coverage. Analysis of the sample from the group that suffers flame-out showed large regions of pure titanium in the interior of the sample and higher levels of oxygen contamination. These oxide regions act as insulators in the material which cause the secondary electron emission to decrease, the plasma current to drop and the voltage to rise. The less dense targets had a surface topography which helped overcome these decreases is electron emission. Experiments showed that an increase in the voltage with respect to the surface significantly increased electron emission, for the less dense targets, counteracting any drops in plasma current.

I. INTRODUCTION

Magnetron sputtering devices are used to deposit thin films in a broad range of applications. A plasma discharge is started between the target and substrate by biasing a high negative voltage to the target, while the substrate and the rest of the chamber remain grounded. It is sustained by ion-induced electrons emitted from the target cathode.[1] This article details the differences in magnetron performance of two types of 90% W–10% Ti magnetron targets. Though specific, the insights gained can be applied to a variety of target-produced magnetron instabilities. Two different density targets, which differed mainly in micro structure, were examined. The less dense target (A) was manufactured from tungsten and titanium powders of 20–200 μm size. It was sintered at 1200 °C with no applied pressure. The other target (B) was made from similar size powders, but was sintered at a lower temperature, 800 °C, with applied pressure of 300 MPa. The densities of the two materials differed: 11.1 g/cm^3 for A and 14.4 g/cm^3 for B. Under this process the maximum theoretical density is 14.52 g/cm^3. Target A had a porosity level of 38% compared to the maximum theoretical density of the material, 17.9 g/cm^3. Target B had a porosity level of 20%.

When the target of lower density (A) was used for sputtering, particulate emission was noticed. After several hours of sputtering, particles of at least 10 μm size were detected on the substrates at a concentration of 1.5 particles/cm^2. Target B was characterized by significantly lower particulate formation rate, 0.07–0.17 particles/cm^2 of the same size as A. The problem of particulate formation has been studied by Wickersham *et al.*[2]

A problem associated with the use of W–Ti targets is a phenomenon known as "flame-out." It is marked by a sudden decrease in discharge current, accompanied by a concurrent rise in the voltage, which occurs erratically. Eventually, the current decrease and voltage increase become so significant, that the magnetron power supply cannot maintain the plasma. Occasionally, the discharge may relight, especially if the system pressure is increased, and sputtering will continue. If the situation reoccurs after reignition, the target cannot be used. Sometimes, a target that has experienced flame-out in one sputtering system will function normally in a different system. The round targets are 50 mm in diameter and 3 mm thick. They were determined to be of high purity by glow discharge mass spectroscopy (600–700 ppm O_2, less than 200 ppm C). Of the two targets tested, target A, the lower density one, did not suffer flame-out problems. The target could be sputtered for its entire lifetime (15 h) without problems. The higher density target (B) did suffer from flame-out, with a typical use of only 3 h before flame-out occurred. The sputtering tests were performed using a system described earlier.[3]

Two techniques were used to determine a possible explanation for the phenomenon: Auger electron spectroscopy (AES) and ion-induced electron emission measurements. Scanning AES was used to obtain scanning electron microscopy (SEM) pictures and elemental composition of the surfaces in question. In addition, the ion-induced secondary electron emission coefficients of the two targets were examined.

II. AUGER ELECTRON SPECTROSCOPY

An Auger electron spectrometer in the Center for Microanalysis of Materials at the University of Illinois was used to image and analyze the atomic composition of three re-

 0734-2101/94/12(4)/1408/9/$1.00

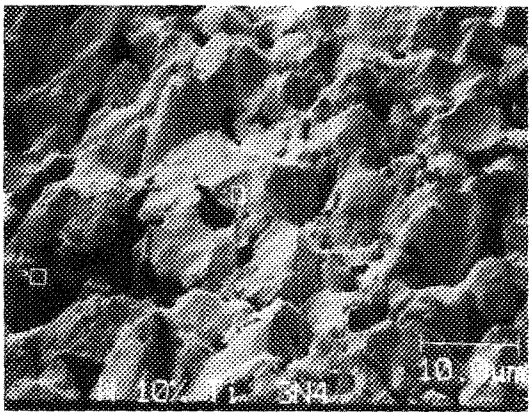

FIG. 1. Porous sample in heavily sputtered region. The indicated regions were analyzed using depth profile.

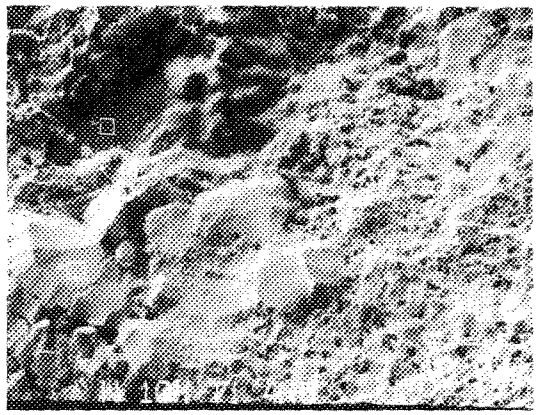

FIG. 2. Flame-out sample in heavily sputtered region. The two areas outlined were analyzed using a depth analysis.

gions of each sample. AES uses the detection of emitted Auger electrons induced with an incident electron beam. The energy of an Auger electron is characteristic of the atom it came from. This allows for atomic composition of an area to be analyzed.[4] By scanning the electron beam over the surface of a sample, an image can be produced. The first area to be examined was in the most heavily sputtered region of the samples. Another area on the sample that had not been subjected to such a high flux, but had been sputtered, was looked at. The third area analyzed was the back of each sample, which is indicative of the unsputtered target surface before being polished.

An area was examined using absorbed current images at magnifications of 200 and 2000 times to learn the different features of each surface. After areas of interest were pinpointed, an atomic composition analysis was performed. As expected, the surface had been contaminated with oxygen and carbon by normal exposure to the atmosphere. Using a 3 keV argon ion beam, the surface was cleaned and then sputtered away to provide a depth profile of the sample. During the profiles, a layer of less than 50 nm was removed, an atomic composition analysis was done, and the process repeated until the concentration of each of the components of an alloy did not change by more than 10%. Final profile depths ranged from 350 to 1600 nm.

In the heavily sputtered region, at a magnification of 2000 times, the differences in surface features between the two samples can be easily seen. The sample which did not experience flame-out (A) is very porous. (Fig. 1) The surface is made up of many similar cones each approximately 5 μm wide. In contrast, the surface of the target more prone to flame-out (B), is multifaceted. (Fig. 2) Its smooth surface has dark regions interspersed in a material of lighter color of two different grain sizes. A dark color is indicative of a low electron-induced secondary electron emission coefficient.

An initial analysis of the three areas outlined in Fig. 1 was performed. The top and side of a cone were examined, along with the deep part of a valley. After a slight argon sputter, the top of the cone was found to have the following composition: 36±5% W and 4.0±1.5% Ti. The rest of the surface was oxygen (12±2%) and carbon (48±6%) contaminants. The side of the cone did not differ by very much. It was found to be 21±3% W and 10±2% Ti. The remainder was carbon (48±8%) and oxygen (21±3%). The initial composition of the valley was identical to that of the top of the cone.

The results of a depth analysis to 1200 nm were identical at both the top of the cone and on the side (Table I): 74±6% W and 7±3% Ti (W:Ti ratio of 10.6). There appears to be little compositional variation between topological features in this region. A similar analysis to 350 nm was done on target B in the regions outlined in Fig. 2. The very dark colored region was found to be rich in titanium characterized by a W:Ti ratio of 0.09. The two lighter colored regions were found to have compositions similar to each other. The W:Ti ratio found in these areas of approximately 7 is closer to the desired composition of the alloy. (Table I) This heavily sputtered region of the surface appears to be much less homogeneous than the same area on target A.

When the two targets were examined in lightly sputtered areas, the same features seen in the heavily sputtered regions were found in the samples again. The image of target A, the porous sample, had lightly colored grains on the surface. The atomic composition of the material was found to be 75±5% W and 8±3% Ti, a W:Ti ratio of 9.4, close to the desired overall mixture. The composition of the alloy is very similar in both sputtered regions. This indicates that sputtering of all materials proceeds at an even rate when the porous sample is used in the magnetron. A dark region of sample B was profiled to a depth of 1600 nm. It was found to be 55±3% W and 28±3% Ti, a W:Ti ratio of 2.0. This is still enriched in titanium, but less than was seen in the heavily sputtered region.

The appearance of the back of the samples differed greatly from the front of the samples due to machining and to the absence of sputtering. Machining removed the peaks of target A, the porous sample. The result is a flat surface with pits of size up to 100 μm in diameter (Fig. 3). A similar flat surface is seen on the back of target B. This sample has no depressions, due to its high density (Fig. 4). Three areas on the back of target A were analyzed after a two minute sputter clean; a dark flat region, a light-colored flat region and an

TABLE I. Atomic concentration analysis in the heavily sputtered region of the samples.

Area examined	Percent tungsten	Percent titanium	W:Ti ratio	Percent oxygen	Percent carbon
Target A[a] (porous)					
Side of cone-1 (before)	36%±5%	3%±1%	12.0	12%±2%	50%±5%
Side of cone-1 (after)	75%±5%	7%±3%	10.7	7%±3%	12%±3%
Top of cone-2 (before)	21%±3%	10%±2%	2.1	21%±3%	48%±6%
Top of cone-2 (after)	73%±5%	7%±3%	10.4	7%±3%	11%±3%
Target B[b] (flame-out)					
Dark area-1 (before)	17%±3%	14%±2%	1.2	23%±3%	46%±7%
Dark area-1 (after)	7%±1%	80%±5%	0.09	6%±2%	6%±2%
Large grains-2 (before)	45%±5%	4%±1%	11.36	13%±2%	38%±5%
Large grains-2 (after)	73%±8%	10%±2%	7.3	9%±2%	11%±2%
Small grains-3 (before)	43%±4%	3%±1%	14.3	17%±3%	38%±5%
Small grains-3 (after)	71%±7%	10%±2%	7.1	8%±2%	13%±2%

[a]The after analysis of target A is at 1200 nm.
[b]The after analysis of target B is at 350 nm.

area in a depression. Table II displays these results. The ratios of tungsten to titanium found in the dark area and inside the depression are less than 1.5, in the light area it is greater than 10, compared to the desired W:Ti ratio of 9.

The back of sample B was also examined. The two areas outlined in Fig. 4, a dark region and a light region, were analyzed before and after a two minute argon clean. Before the surface was cleaned, the dark region contained no tungsten and was almost 75% carbon. The light region did contain some tungsten, but still had a high carbon content, 57%. (Table II) After the surface had been cleaned, carbon levels had dropped significantly. The carbon present after cleaning made up 11% of the dark region and was not found in the light region. Still, no tungsten was found in the dark area. The tungsten content of the light area shot up to 89% giving a W:Ti ratio of 22.3.

Target A, the porous sample, is more homogeneous than target B on the back of the samples. In the case of flame-out (target B), the dark region was found to be almost pure titanium, no tungsten at all. Although areas rich in titanium and areas rich in tungsten were found on the unsputtered back of the porous alloy, it appears that all elements are sputtering at equal rates. There seems to be no change in the composition of the alloy as sputtering progresses. The proportions of the two elements are near the intended levels, and the target is sputtering evenly. The other alloy is not as homogeneous.

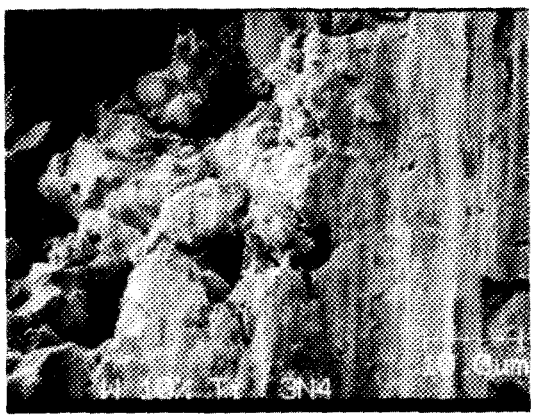

FIG. 3. The unsputtered back of the porous sample. The areas analyzed with depth profile are too spread out to be pictured here.

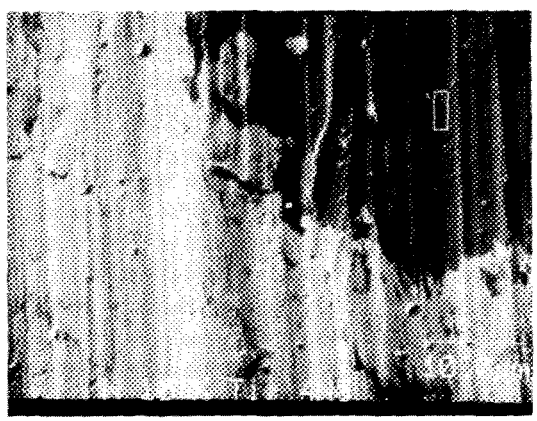

FIG. 4. Flame-out sample on the back of the target. The two areas outlined were analyzed using depth analysis.

TABLE II. Atomic concentration analysis from the back of the samples.

Area examined	Percent tungsten	Percent titanium	W:Ti ratio	Percent oxygen	Percent carbon
Target A[a] (porous)					
Dark area	14%±3%	42%±8%	0.3	36%±6%	9%±2%
Light area	73%±7%	7%±1%	10.4	10%±2%	10%±2%
Depression	26%±4%	24%±4%	1.1	16%±3%	34%±6%
Target B[b] (flame-out)					
Dark area (before)	···	17%±2%	···	11%±2%	72%±8%
Dark area (after)	···	79%±7%	···	11%±2%	11%±2%
Light area (before)	10%±1%	11%±2%	0.9	21%±3%	57%±8%
Light area (after)	89%±6%	4%±1%	22.3	7%±1%	···

[a]The composition of target A was analyzed after a cleaning sputter.
[b]Target B was analyzed before *and* after a 2 min sputter with an argon ion beam.

Mixing of the material is usually better, but inter diffusion between components is not as complete due to the lower temperature of sintering. Nucleation sites develop in the material that lead to high concentrations of titanium. Regions of almost pure titanium are found on the back of the sample, surrounded by material of higher than desired tungsten content and a small amount of titanium.

The most important difference discovered during the AES study is the depth at which carbon and oxygen fall to negligible levels. This difference in contaminant level can be observed by comparing the depth analyses of the two samples in the lightly sputtered regions. Figure 5 is the composition analysis of target A to a depth of 575 nm. At the first point recorded after the initial analysis (20 nm), the percentage of the material that is carbon has already dropped to its final level. For contrast, the analysis of a dark area of target B is pictured in Fig. 6. This profile goes much deeper, 1600 nm. The contamination of carbon and oxygen extend much farther into the material. Oxygen dies away in 200 nm, while the carbon is present in elevated quantities to a depth of approximately 400 nm. This same phenomenon was seen in all profiles. The contamination level dropped immediately in target A, but remained to a greater depth in the other sample.

Under certain sputter conditions, when the residual gas flux to the sputter surface is not negligibly small compared to the argon and ion fluxes, plasma activated surface oxidation may occur. This oxidation is accompanied by diffusion of residual gas species into the target material because of the

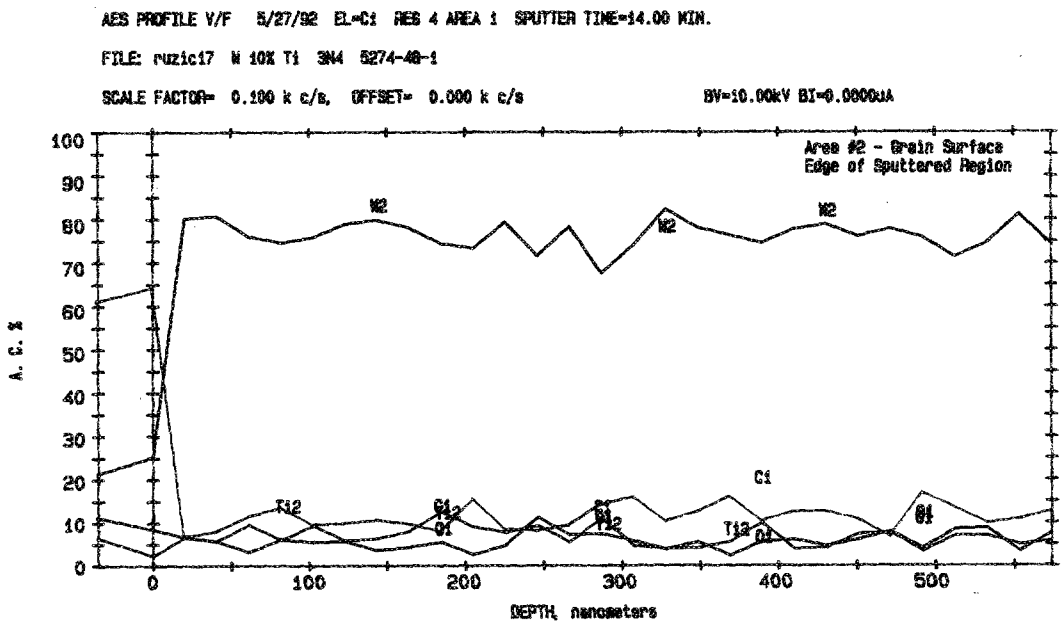

FIG. 5. Depth analysis, to 575 nm, of a dark area in the lightly sputtered region of target A (porous target).

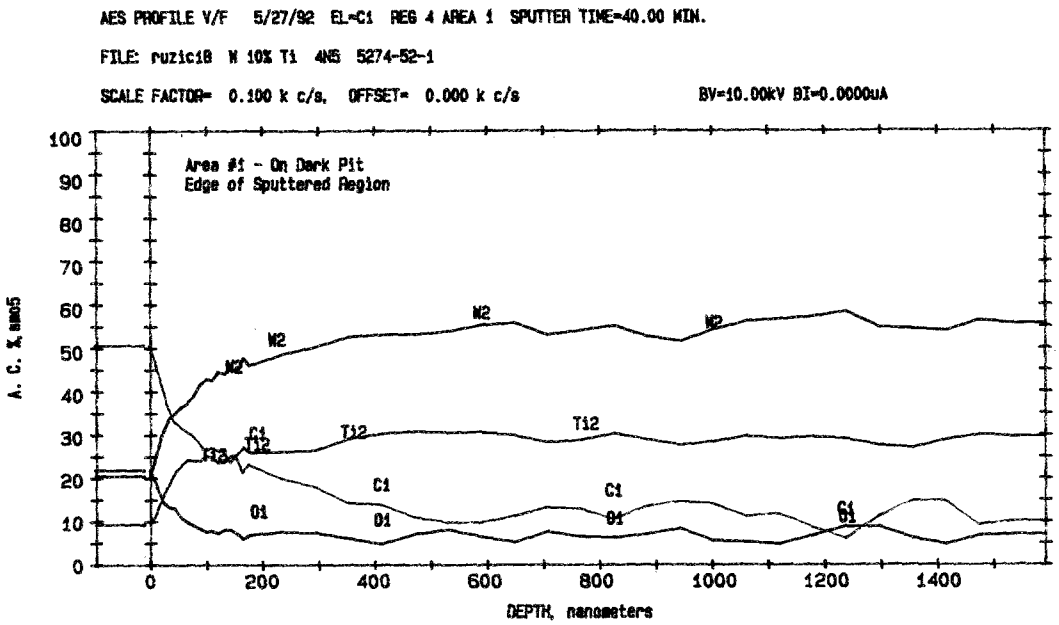

FIG. 6. Depth analysis, to 1600 nm, of a dark area in the lightly sputtered region of target B (more prone to flame-out problems).

difference in concentration of these species between the surface and the interior of the target. The extent of oxidation is affected by the topography of the surface. Because target A has a rougher surface than target B, the level of oxidation per unit surface area observed is expected to be lower in target A. This relation was seen in the AES studies. These oxides act as insulators reducing electron mobility. When electrons are emitted from a grain with an oxide layer, it is difficult for other electrons to move into that area to replace those that are lost. This decreased electron mobility reduces the overall electron emission of the surface.

III. ION-INDUCED SECONDARY ELECTRON EMISSION

Because application of a high voltage to maintain the plasma in a magnetron is undesirable, the ion-induced secondary electron emission coefficient, γ, of a magnetron target becomes an important parameter. High voltage leads to high energy ions, which create very energetic particles that sputter the substrate surface instead of being deposited on that surface. To avoid this problem, the electron emission must be high, so the target can contribute sufficient electrons to sustain the plasma at low ion energies. In this study, the ion-induced secondary electron emission was examined for both samples under various conditions. A comparison between the two samples was made using both 700 eV helium ions and 700 eV argon ions. The back of each sample, where no sputtering had occurred, was compared to regions on the front, that had been sputtered. This experimental set-up maintains an equal potential on both the target and on the collection cylinder.

In addition, an attempt to simulate the effect of the magnetron plasma sheath was made by placing a positive bias of 93 V on the cylinder used to collect electrons. Inside a magnetron, the plasma sheath, a potential gradient usually less than one mm thick, is able to wrap around the larger scale surface features of the sputtering target. This potential accelerates electrons into the plasma and may increase emission. In addition, field emission at sharp surface protrusions also contributes to higher electron emission. By using a positive potential bias on the collection cylinder, a greater percentage of the electrons that are actually emitted by the target surface are pulled away from the target, theoretically allowing a more accurate reflection of the emission characteristics of the target in a magnetron.

The helium and argon ions are produced in a Colutron, plasma-based, ion gun. The ions are extracted with a Einzel lens at energies ranging from 700 to 1000 eV. The ions then travel through a series of lenses and filters on their way to the target assembly. An $\mathbf{E}\times\mathbf{B}$ filter is used to mass select the desired ion specie. The beam is then steered through a 5° bend by electrostatic plates to strip any unwanted neutrals. A set of horizontal and vertical raster plates is the next stage of the path. The raster plates can sweep the beam in a square pattern minimizing any inconsistencies in the beam cross section. The last set of lenses is used to decelerate the beam to the desired energy and focus once more. This is done as close to the target as possible to minimize any spreading of the beam that occurred during the trip to the main vacuum chamber.

The target assembly is a system of three stainless steel coaxial cylinders, surrounded by a screen mesh that ensures the beam enters a field free region. The three cylinders each have specific functions in the data acquisition process. They are separated from each other by Teflon spacers and are individually connected to switches that allow their signals to be observed on several pieces of equipment. A hole, of diameter 2.54 mm, in the outer cylinder is used to collimate and focus the beam. By adjusting the voltages on the focusing lenses to minimize the amount of current on the outer

cylinder, a small beam of 0.2–0.4 mm can be produced. The middle cylinder has a hole in line with that on the outer cylinder. This cylinder is used to collect the electrons emitted from a sample when the ions strike the surface. The inner cylinder holds the mounted targets. There are two sites for samples that have these holes over them. Two other locations have long slits that can hold two samples. These slits allow changing from one sample to the other by a simple translation of the target assembly, not the ion beam.[5]

The ion-induced secondary electron emission coefficient γ is the ratio of the number of electrons emitted I_e to the number of incident ions I_i

$$\gamma=\frac{I_e}{I_i}. \tag{1}$$

The current measured on the inner cylinder is due to both incident ions and departing electrons.

$$I=I_i+I_e. \tag{2}$$

There is a percentage of the electrons emitted that will be lost through the hole in the middle cylinder for the ion beam. The real electron current is then higher than the current detected by the middle cylinder M. The correction factor, which is always greater than one, can be calculated and is given the symbol g.

$$I_e=gM. \tag{3}$$

Substituting these in Eq. (1) gives the following expression for γ:

$$\gamma=\frac{gM}{I-gM}. \tag{4}$$

The value of g is dependent on the set up of the experiment, in particular, the bias on the collection cylinder.

The preceding analysis does not address the effect of reflected neutrals: ions that have been neutralized by contact with the target surface and reflected. This phenomenon can have a large impact on γ at low bias voltages. Some reflected neutrals strike the collection cylinder and cause electron emission. The electrons that leave the cylinder result in a less negative signal from the collection cylinder. The electrons strike the target cylinder and lower its positive signal. When a high positive bias is placed on the collection cylinder, this effect is not a problem. All electrons emitted by the collection cylinder due to the reflected neutrals are forced to return to the collection cylinder, cancelling the positive charge caused by their emission.

In the case where no bias is applied to the collection cylinder, both target and collection cylinder are at the same potential, the calculation of g is straight forward. The electrons are emitted in a cosine distribution with respect to the surface normal,[6] and the fraction of electrons that escape through the hole for the ion beam, esc, is easily calculated.[5] From this, $g=1/(1-\text{esc})$ can be determined. With a bias on the collection cylinder, two questions must be answered: (1) will electrons that used to escape now be collected? and (2) will electrons that were collected now escape?

In order to answer those questions, the trajectories of emitted electrons was calculated. It was assumed that a constant electric field parallel to the target E_y was maintained (Fig. 7). The approximation of two parallel plates for the collection cylinder and target was found to be good by comparing this situation with the true set up of a flat target and a curved collection plate. The radius of curvature is large compared to the distance between the target and collection cylinder. Thus, the curvature is insignificant.

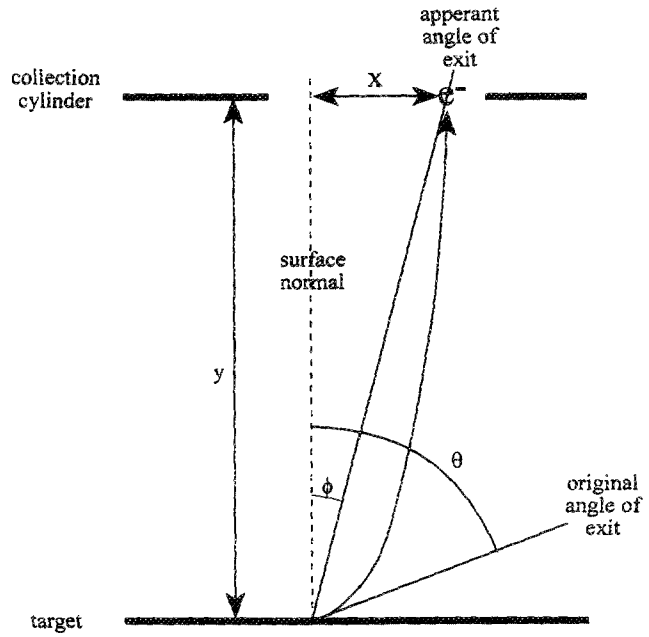

FIG. 7. The effect of the electric field on emitted electrons.

The motion in the y direction is governed by the following equation:

$$y=v_0(\cos\ \theta)t+\tfrac{1}{2}a_y t^2, \tag{5}$$

where v_0 is the initial velocity of the electron when it leaves the surface, θ is the angle (measured from the surface normal) at which the electron leaves the surface, and a_y is the acceleration of the electron in the y direction due to E_y, the electric field. The initial velocity of the electrons was calculated from the assumption that all electrons leave the surface with an energy of 2 eV. Motion in the x direction is as follows:

$$x=v_0(\sin\ \theta)t. \tag{6}$$

Since y, the distance between the target and the collection cylinder, is known, the displacement of an electron, in the x direction, from its point of exit from the surface, can be determined by combining Eqs. (5) and (6). With this information, the apparent angle of exit can be calculated. For example, an electron that leaves the surface at 20° passes the plane of the collection cylinder at an apparent angle of 3°. The electric field bends the flight of the electron toward the surface normal.

Near the hole, the electric field is not parallel to the target surface. There is a bend in the field due to the edges of the hole. The component of the electric field perpendicular to the target surface in this region had a negligible effect on few electrons compared with the effect of E_y. Therefore, the an-

swer to the first question is no; very few electrons that had escaped when the whole assembly was at the same potential are collected when the bias is put in place.

To determine the fraction of electrons escaping collection, a new distribution of electrons based on the apparent angle of emission, ϕ was calculated from Eqs. (5) and (6)

$$\tan \phi = \frac{x}{y} = \frac{v_0(\sin \theta)t}{v_0(\cos \theta)t + \frac{1}{2}a_y t^2}. \tag{7}$$

Assuming that t, the time required to reach the collection cylinder, is constant for all electrons, θ, the original angle of exit, can be expressed as a function of ϕ, the apparent angle of exit

$$\theta = \theta(\phi)$$
$$= 2 \arctan\left(\frac{2v_0 \cos \phi - \sqrt{4v_0^2 - a_y^2 t^2 + a_y^2 t^2 \cos^2 \phi}}{(\sin \phi)(-2v_0 + a_y t)}\right). \tag{8}$$

The samples tested here were mounted on slit positions. For this case, the following expression is the formula for esc, the fraction of electrons that escape through the hole in the middle cylinder and are not collected.

$$\text{esc} = \left[\int_b^a dx \int_0^{\arctan\left(\frac{w-x}{y}\right)} \cos[\theta(\phi)]\, d\phi\right] \Bigg/ \left(\int_b^a dx \int_0^{\phi'} \cos[\theta(\phi)]\, d\phi\right), \tag{9}$$

where w is the width of the slit, the length ab is the width of the beam hitting the surface, and ϕ' is the value of ϕ where θ is 90°.

When no bias was applied, the fraction of electrons that escape, esc, was 24% for target A, and 23% for target B. More electrons escape when target A is tested because it is thicker. Thus, its surface is closer to the collection cylinder, so the solid angle subtended by the hole is larger. When a +93 V bias was placed on the collection cylinder, esc was 89% for target A and 88% for target B. The answer to the second question, then, is yes—many electrons now escape that used to be collected. The geometrical correction factor, g, defined as $1/(1-\text{esc})$, accounts for these escaping electrons in Eqs. (3) and (4).

The calculations of g were checked by measuring the number of electrons collected as a function of bias voltage for a gallium–arsenide target. A gallium–arsenide target was used because its flat surface would eliminate variations due to field emissions of surface peaks that are present in other materials. As the voltage on the collection cylinder is increased the calculated g factor also increases since more electrons escape through the hole in the collection cylinder. This calculated g factor (shown numerically below each data point in Fig. 8) is then used to calculate a γ from the data. If the calculations are correct a constant value of γ as a function of collection voltage should result.

Figure 8 indeed does show an approximately constant value of 0.2 after at least 30 V are applied. The difference between the value of γ at no bias and the value of γ at higher

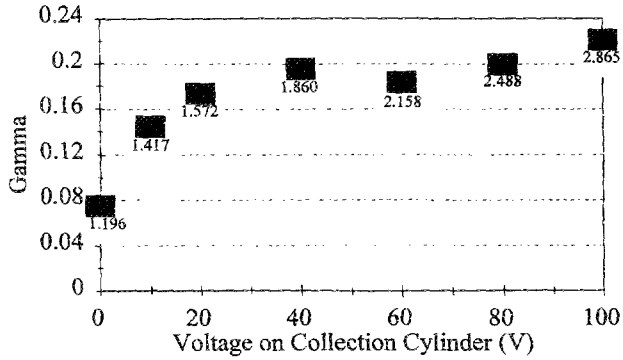

FIG. 8. γ of gallium–arsenide as a function of bias on collection cylinder. Values beneath data points are the calculated g factors.

voltages is due to the effect of reflected neutrals. Some ions strike the target and reflect as neutral atoms. Upon striking the collection surface they can cause electrons to be emitted. A rise in the voltage of the collection cylinder with respect to the target returns these electrons to the collection cylinder thereby increasing the measured value of γ.

The sources of error in a value for the electron emission coefficient include the geometric correction factor, and errors in the values of current read on the ammeter. These errors are machining errors, zeroing error, reading error, signal variation, and inherent meter error. When all of these sources are considered, an error of 5%–15% was calculated for each value of γ for the case where no bias is applied to the collection cylinder.[5]

For the case of a bias applied to the collection cylinder, other sources of error arise: the true bias applied to the collection cylinder, the average time required for each electron to reach the plane of the collection cylinder, and the average energy of the emitted electrons. The uncertainty in the average energy of the electrons is the overwhelming source of error in the value of g. The calculation performed for this analysis considered the energy of the emitted electrons to be 2.0 eV. When calculations using 1.8 and 2.2 eV were done, the value of the geometrical correction factor, g, ranged from 5.3 to 13.3. Because the true energy of the electrons emitted is not known, the absolute magnitude of γ cannot be determined with much certainty. Since the energy spectra of the emitted electrons will be the same for both samples, the relative magnitude of γ for the two will be unaffected by the variation in g.

A typical data run consisted of putting the beam on target in the desired location. At regular intervals of one or two minutes, the current on the inner cylinder was read. Then, the current on the middle cylinder was recorded. The current on the inner cylinder was recorded again, to determine variations in the beam intensity. From this, a graph of γ as a function of time was obtained.

Immediately after exposure to the ion beam, the value of γ decreases rapidly. This change in γ corresponds to a change in the layer of adsorbed gases on the surface of the sample, as the ion beam removes some of this adsorbed gas. Data is taken until there is variation of less than 1% in the

TABLE III. 700 eV He^+ induced electron emission coefficients.

Area examined	Target A	Target B
Heavily sputtered region	0.095±0.008	0.162±0.018
Lightly sputtered region	0.084±0.008	0.146±0.017

value of γ for at least 3 min. The stable readings are used to compute an average value of γ. This is used as the electron emission coefficient of the particular sample at that particular location.

As was mentioned, the sputtered regions and the back of each sample were examined. In addition to targets A and B, another target, B1, from group B was mounted in the target assembly. This target had been polished, but had not been sputtered. This was a sample that had been tested previously, and was used here to determine reproducibility of measurements and to allow comparisons with other 90%W–10%Ti samples.

The two different sputtered regions on each target, examined during the AES tests, were tested with 700 eV helium ions with no bias voltage placed on the collection cylinder. Helium was used to enable easy comparison to other targets. No difference was seen between the heavily sputtered and lightly sputtered regions on a sample. The values of γ from helium ions for target A (porous) were consistently lower than those for target B when target and collection cylinders were at the same potential (Table III). These values of γ should not be considered as absolute values, since the original analysis did not involve the effect of reflected neutrals. When this is taken into account, the values of γ will be higher. However, the values quoted here, relative to one another, are still valuable. The difference between the two samples is explained by considering the surface characteristics of the two samples. The porous sample, having more peaks and valleys, does not allow as large a percentage of the emitted electrons to escape and be collected. More electrons are obstructed due to the surface features. Since the fraction of emitted electrons that are collected M is lower, the resulting value of γ is falsely low; the numerator of the expression for γ is gM. Both of these targets had values of γ that were lower than the value for the polished target B1 which was 0.199±0.016. This was expected since the surface of this sample was more smooth, allowing more electrons to escape the surface and be collected.

The same tests were run on the samples using 700 eV argon ions. During these tests the sputtered surface of both targets was compared with the back of each sample. In addition to these experiments, where the collection cylinder and target are at the same potential, tests were performed with the collection cylinder at +93 V with respect to the target to mimic more closely the conditions in a magnetron by pulling more electrons from the surface of the target (Table IV). Again, the unbiased cases do not consider the effect of reflected neutrals.

TABLE IV. 700 eV Ar^+ induced electron emission coefficients.

Area examined	Target A (porous)	Target B (more smooth)
Sputtered, no V_{accel}	0.005±0.001	0.018±0.002
Sputtered, V_{accel}=93 V	0.218±0.074	0.242±0.090
Unsputtered/unpolished	0.050±0.004	0.064±0.004

When no potential is applied, γ for target B is approximately three times higher than the value of γ for the porous sample in the sputtered areas. The same phenomenon was seen when helium was used. It is due to the difference in surface topography between the two targets. When the bias was applied to the collection cylinder, the calculated values of γ for the two samples increased to the same level at 21.8%±7.4% for target A and 24.2%±9.0% for target B. The emission of target A did not remain at 30% of the emission of target B. The absence of any difference between the two, in this case, is again explained by the surface characteristics of each target. The porous sample emits more electrons per incident ion. However, during the first experiment, few electrons are able to escape the peaks of the surface when they enter the field free region just above the surface. When the whole target assembly is at the same potential, collection of more of the electrons emitted is possible from target B than is possible from target A. The more dense, less porous material of target B has fewer surface features to obstruct the electrons' paths. When the bias was applied to the collection cylinder, electrons are effectively pulled away from the surface. In the magnetron, the plasma sheath is thinner than the distance between the target and the collection cylinder, and has a larger total gradient across it, further enhancing electron collection by the plasma. This effect of the surface features of a target on the electron emission to the plasma was studied by Leybovich *et al.*[3]

IV. CONCLUSIONS AND DISCUSSION

AES and direct measurement of the ion-induced secondary electron emission of the samples in various regions allow us to explain the cause of the flame-out problem. AES revealed a porous surface on the face of target A. The composition of this target appeared to be fairly homogeneous; the tungsten and titanium are well mixed. The targets from group B (more prone to flame-out) did not have the same topography. These samples are more dense, and have a smoother surface. The composition of this target was less homogeneous. Large deposits of almost pure titanium were found imbedded in material rich in tungsten.

Another feature of target B, discovered using AES, was the greater depth to which contaminants are able to penetrate the surface. In all depth analyses of target A, carbon and oxygen levels were at noise level at all depths except the surface. With the first sputter clean, these elements disappeared. In contrast, carbon and oxygen existed at substantial levels much farther into the material of target B. This high contamination level has lead to larger regions of oxide that act as insulators, reducing the mobility of electrons and in turn the electron emission of the surface.

The emission characteristics were also examined. When the target and the collection cylinder are at the same potential, the fraction of emitted electrons collected from target B was higher than the fraction collected from target A. This led

to a higher value of γ for the flame-out sample. This difference in the fraction collected is due to the difference in the surface features: the porous sample (target A) has more cones and valleys. Therefore, a significant portion of the electrons are captured by the surface and never collected when no bias is applied to the collection cylinder. When the collection cylinder was biased positively 93 V with respect to the target, a greater number of the emitted electrons are captured, reducing the effect of the differences in the surface topography.

In the environment of a magnetron, a stronger electric field is present, which allows the electrons emitted to be pulled into the plasma and help sustain it. Under the high potential, the secondary electron emission coefficient of sample A would be higher than the emission coefficient of sample B after some sputtering has occurred. Therefore, the flame-out phenomenon can be explained in the following manner. Initially, the secondary electron emission coefficient of target B is enough to sustain the plasma. As sputtering proceeds, the exposure to residual gas species causes oxide growth. At a certain thickness, the oxide can act as an insulator, causing electron mobility to decrease and γ to fall. When the electron emission drops, the plasma potential increases to compensate. The increased potential induces an elevated electric field in the oxide layer. This may cause an electrical breakdown destroying part of the oxide. γ will increase and the plasma can be restored. However, further exposure to residual gas may cause oxide recovery and γ drops again. In cases where flame-out does occur, the oxides are not destroyed and the electron emission coefficient drops so low that the plasma cannot be maintained and is extinguished. When the plasma recovers from the oscillations to sputter normally, enough electrons have reached the surface to return electron emission to higher values. In the case of target A, field emission from peaks covered by oxide is able to generate hot electrons that get through the oxide and flame-out does not occur. In addition, the porous structure of target A allows even more emission as the potential increases, thus self-correcting any tendency toward an $I-V$ oscillation.

ACKNOWLEDGMENTS

A portion of this work was carried out in the Center for Microanalysis of Materials, University of Illinois, which is supported by the U.S. Department of Energy Grant No. DEFG02-91-ER45439. This work was also supported by the Department of Energy, Contract No. DOE-ANL-2044-2401 and by a gift from Tosoh SMD Inc., Grove City, OH.

[1]S. M. Rossnagel, in *The Handbook of Plasma Processing Technology* (Noyes, Park Ridge, NJ, 1990).
[2]C. E. Wickersham, Jr., J. E. Poole, and J. J. Mueller, J. Vac. Sci. Technol. A **10**, 1713 (1992).
[3]A. Leybovich, T. Kuniya, P. C. Smith, M. B. Hendricks, and D. N. Ruzic, J. Vac. Sci. Technol. (to be published).
[4]D. P. Woodruff and T. A. Delchar, Woodruff and T. A. Delchar, *Modern Techniques of Surface Science* (Cambridge University Press, Cambridge, 1986).
[5]P. C. Smith, M. S. thesis, University of Illinois, Urbana, IL, 1993.
[6]R. C. Abbott and H. W. Berry, J. Appl. Phys. **30**, 871 (1959).